Volume 11, 181-202 (2008) **HYDROACOUSTICS**

EXPERIMENTAL EVIDENCE FOR ENHANCED TARGET DETECTION BY SONAR IN BUBBLY WATER

TIMOTHY LEIGHTON, DANIEL FINFER, PAUL WHITE

Institute of Sound and Vibration Research, University of Southampton,
Highfield, Southampton SO17 1BJ, UK
Corresponding author: tgl@soton.ac.uk

A sonar system has been developed which allows one to discriminate targets from scattered energy from bubbles. The underlying theory and experimental testing of this system are presented. The effectiveness of this sonar system is demonstrated through experimentation within a large fresh water tank in which bubble clouds are generated. Some of the practical requirements associated with such an experiment are detailed.

INTRODUCTION

Following its proposal in 2004 [1, 2], the hypothesis that Twin Inverted Pulse Sonar (TWIPS) could enhance target detection in bubbly environments has been supported through simulation [3-6] and tank tests [7-9]. The principle of operation is shown in the thought-experiment proposed in Figure 1. In this, one wishes to use sonar to detect a linear scatterer, given that there is a bubble cloud in the propagation path. Such a linear scatterer might be a fish, with or without a swim bladder (which at sufficiently high frequencies would behave linearly[†]) within a dolphin bubble net. If amplitude of the insonifying field were to be high enough to generate a nonlinear response, it might be possible to enhance scatter from the linear scatterer, whilst simultaneously suppressing it from the bubbles. Consider an insonifying field consisting of two high amplitude pulses, one having reverse polarity with respect to the other (Figure 1, top line). Linear reflection from the linearly scattering body (which we shall call the 'solid') is shown in b(i). The bubble generates nonlinear radial excursions (Figure 1 a(i)) and emits a

[†] Note that, if one drove the swim bladder at resonance in an attempt to detect the fish amongst linear clutter (including any linearly scattering bubbles), the P_+ solution shown in Figure 1 could be used.

corresponding pressure field (Figure 1 a(i)) (the relevant time histories can readily be calculated [6]). Normal sonar may not be able to detect the signal from the solid (Figure 1 b(i)), as it is swamped by that from the bubbles (Figure 1 a(ii)).

The data are processed through combination of the return signals from the two TWIPS pulses. By adding the two returns, the resulting signal being termed P_+, the scattering from the bubble is enhanced (Figure 1 a(iii) and a(iv)), whilst the scatter from linear scatterers (such as a solid object) is suppressed (Figure 1 b(ii)). In biomedical applications this can be used to enhance the scatter from contrast agents [10, 11]. If however the two halves of each returned signal are subtracted from one another, to form P_-, the scattering from the bubbles is suppressed (Figure 1 a(v) and a(vi)) whilst the reflections from the solid body are doubled (Figure 1 b(iii)). The formation of P_+, or the formation of P_-, is termed TWIPS1.

Insight into the functioning of TWIPS can be obtained by expanding the pressure time series emitted by the bubble in terms of a power series as illustrated in Figure 1. Whilst the addition function of P_+ effectively eliminates all the of linear scatter, it also enhances the even powered terms in the bubble scatter. In contrast the formation of P_- is not so efficient at providing discrimination: it only suppresses part of the nonlinearity (the even terms) and, just as it enhances the linear scatter from the target, it also enhances the odd-powered terms in the scatter from the clutter. In such circumstances, it may be necessary to use TWIPS2, constructed by forming the ratio P_- / P_+, to provide adequate discrimination. Of course the generation of such ratios, particularly when the small value of the denominator is formed through the subtraction of two noisy large values, is prone to oversensitivity due to the effect of noise.

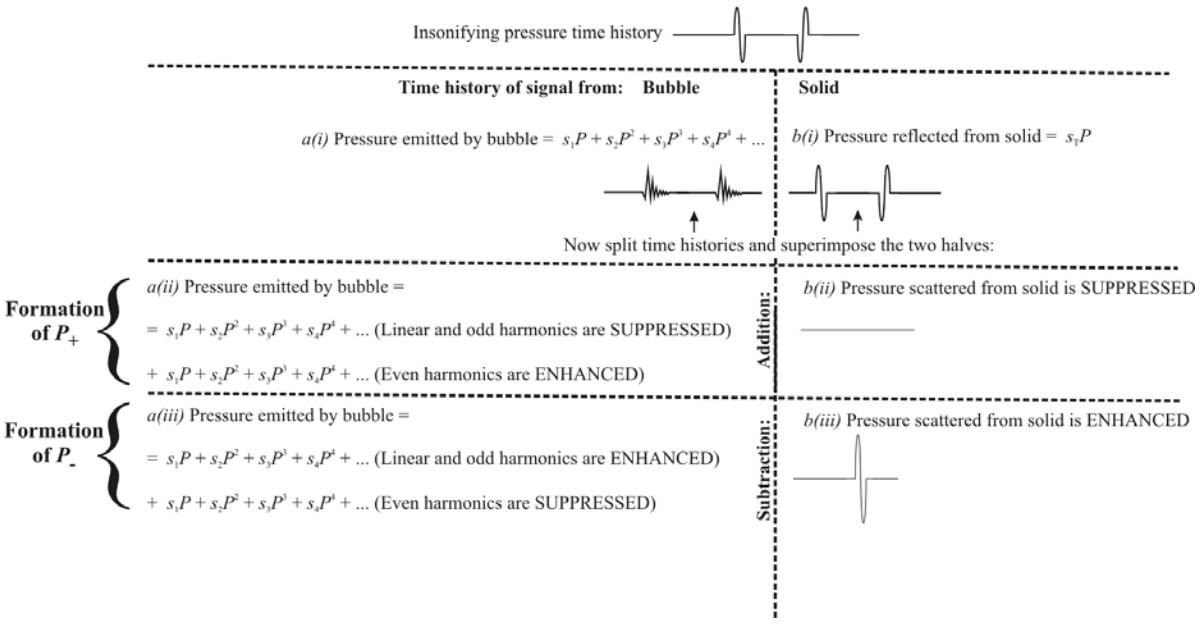

Figure 1. Schematic of the formation of P_+ and P_-

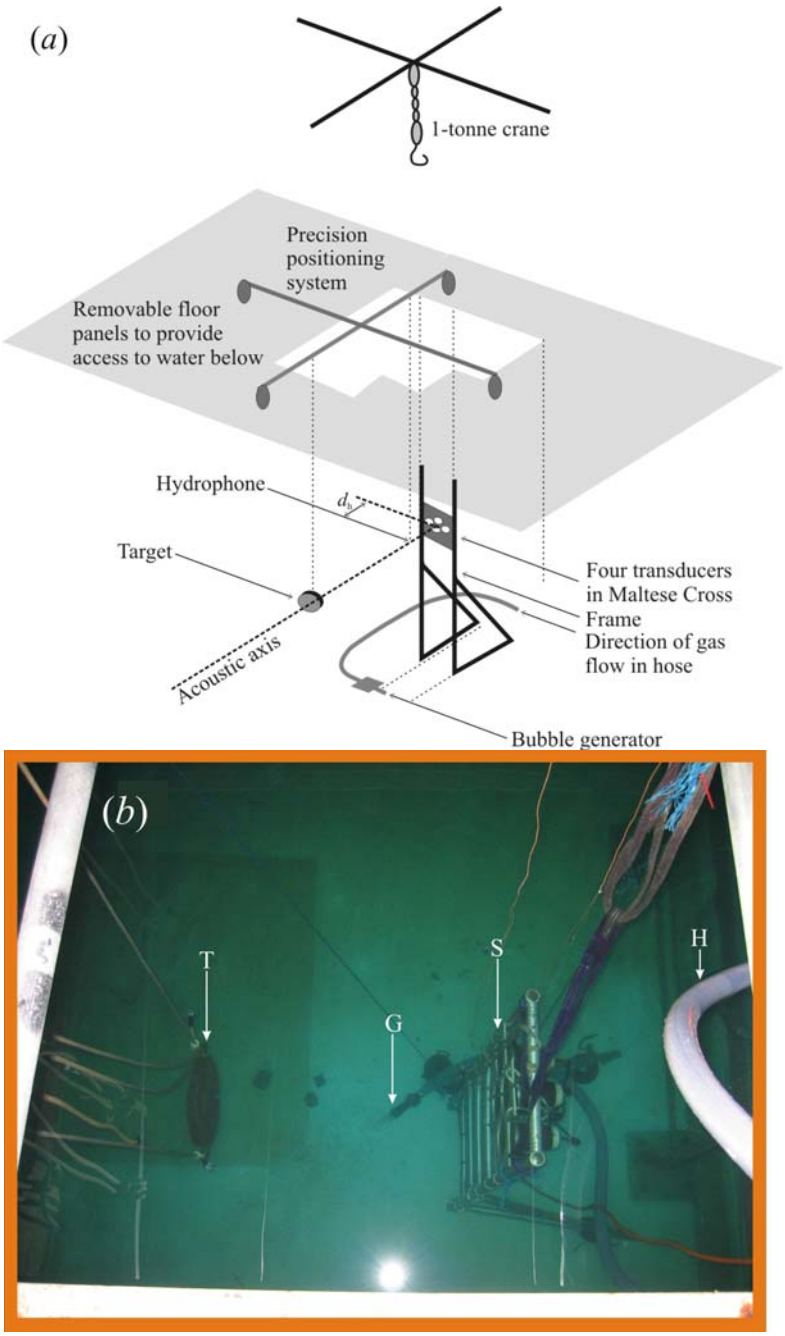

Figure 2 (a) Schematic of proof-of-principle TWIPS experiment. Below the floor (shown shaded) is an underground water tank, 8 m × 8 m × 5 m deep (ISVR's A. B. Wood tank). A rigid frame holds 4 transducers in a Maltese Cross, A hydrophone and a target are aligned on the horizontal acoustic axis, the hydrophone behind d_h=0.10 m in front of the source faceplate. (b) Photograph looking down into the water. Target (T) is 2 m from source (S). Hose (H) feeds bubble generator (G).

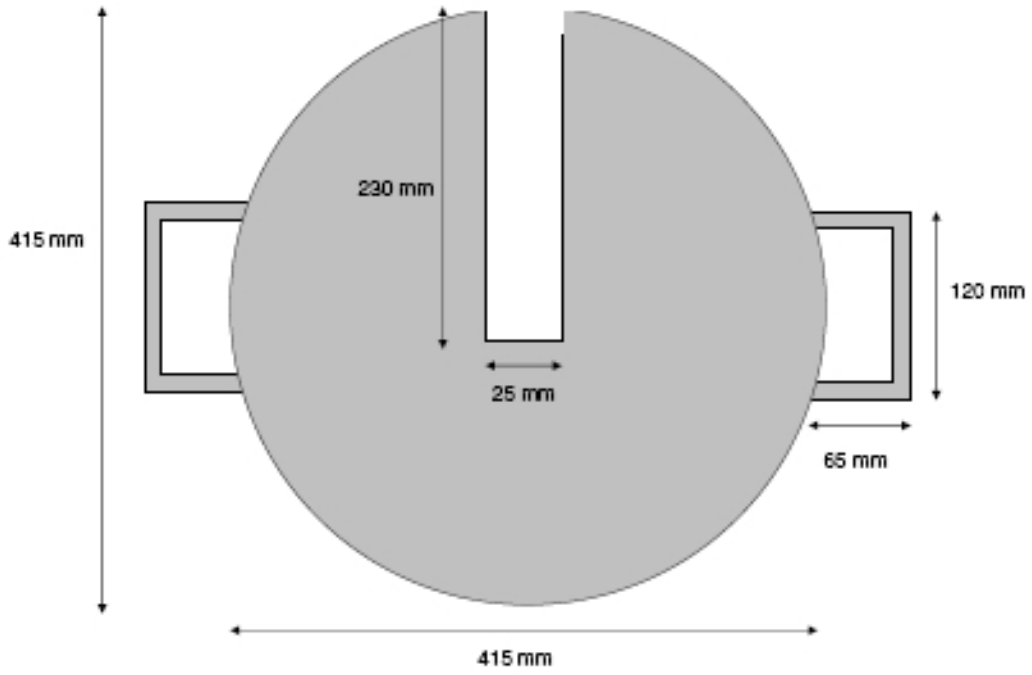

Figure 3. The target used for the TWIPS experiment (a weight-lifter's weight).

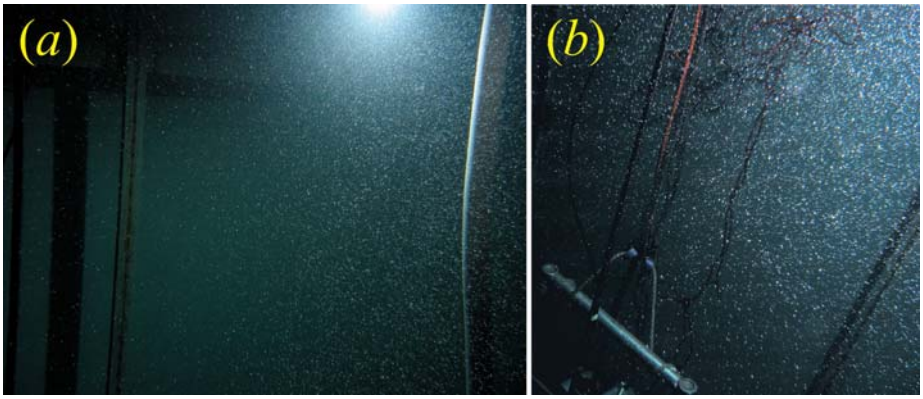

Figure 4. (a) This image shows the bubble cloud used during one TWIPS test. The section of wall visible in the background of the photo measures ~3.3 m × 2.5 m, and is at a distance of 3 m from the camera location. The bubble cloud is distributed into the water column by a diffuser located halfway between the camera and the wall. The hose (white, at right), is 5 cm in diameter, and is along the approximate centreline of the cloud, at a distance of 1.5 m from the camera location. (b) Photograph from the top of the water column, showing the scaffolding bar at the top of the frame which holds the source. That bar is at a depth in the water of 2.03 m, and its length is 0.8 m.

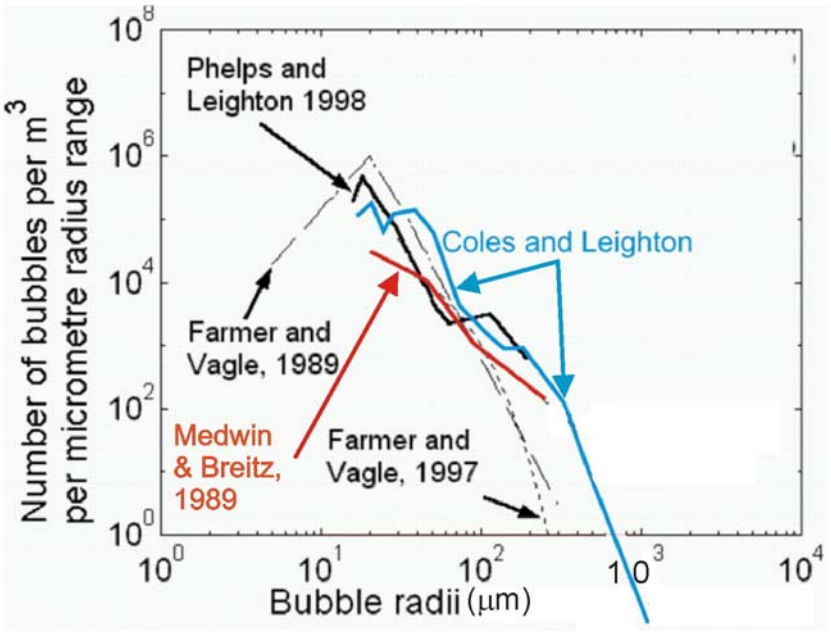

Figure 5. The bubble size distribution used in the experiment is labelled Coles and Leighton [12]. It compares well with a range of bubble populations measured at sea, by Farmer and Vagle [13, 14] and Medwin and Breitz [15].

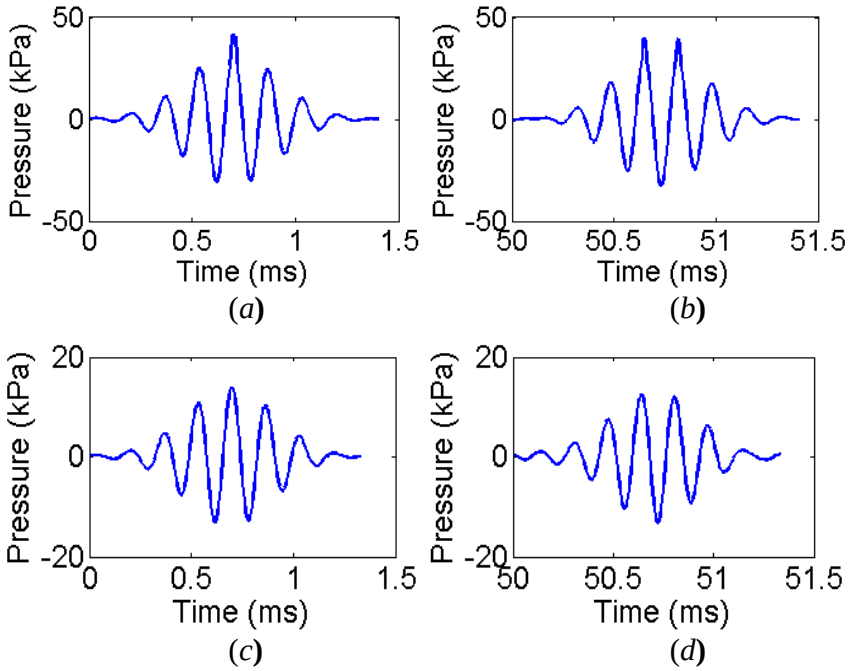

Figure 6. The TWIPS pulses used in this paper, recorded in the test tank in the absence of bubbles. (a) First half of out-going signal at a distance of 1 m from the source. (b**)** Second half of out-going signal at a distance of 1 m from the source. (c**)** First half of outgoing pulse as measured at target location. (d**)** Second half of outgoing pulse as measured at target location.

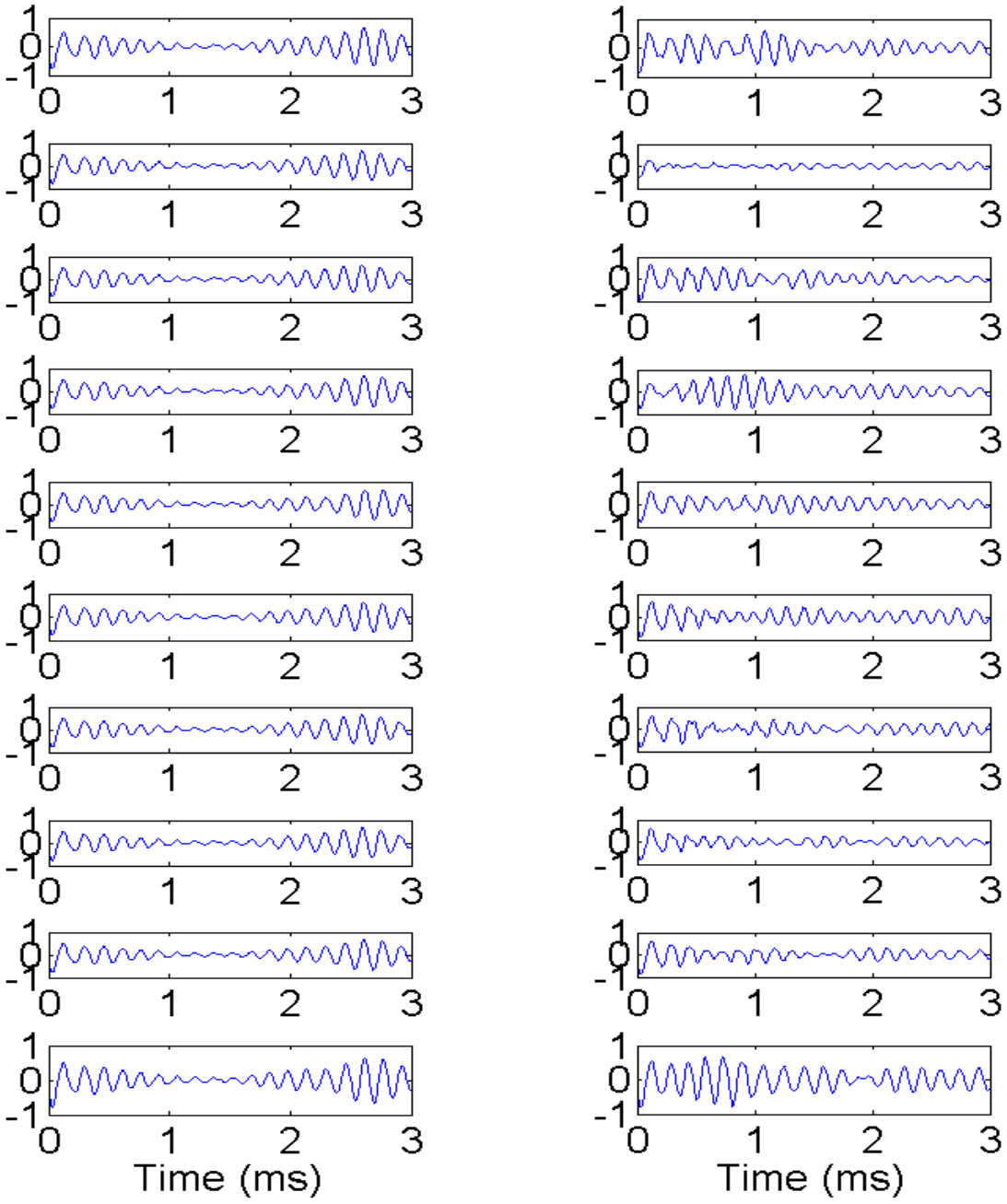

Figure 7. The effect of bubble scattering on target detectability for the first of the pulses in a number of TWIPS pairs. On the left are shown 10 echolocation traces taken in ISVR's A.B. Wood tank in the absence of bubbles. The target is clearly visible as a high amplitude region between 2.5 and 3 ms (the outgoing pulse is visible in the hydrophone signal between time 0 and 1 ms). On the right are shown 10 traces in the presence of bubbles. The bubbles add clutter and variability to the signal between 0 and 3 ms.

2. METHOD

Figure 2 shows the apparatus layout for the detection experiments. The target (shown in Figure 3) was a steel disc of diameter 415 mm and thickness 50 mm. Its calculated target strength is -10 dB for the orientation used in this experiment. It was suspended 2.6 m in front of a sonar source, along the acoustic axis of that source in a horizontal plane and at depth of 2.5 m in the fresh water tank. A monitor hydrophone is also placed on that axis, 10 cm in front of the source, and was used to collect all the echoes reported in this paper. The bubble cloud generator generated a steady cloud of bubbles which occupied an area measuring approximately 2.5 m (cross-beam width) × 1 m (length) in the region situated directly between the source and the target (Figure 4). The bubble size distribution and void fraction resembled that found in the ocean (Figure 5). The outgoing waveform consisted of two pulses generated 20 ms, 50 ms, or 100 ms apart, the second pulse having reversed polarity with respect to the first. Figure 6 shows the acoustic pulses which make up the outgoing TWIPS pulse: the pulses remained the same through the study presented in this paper, although the separation interval between them was varied (a 50 ms separation is used for the examples shown in Figure 6). The waveforms in Figure 6 were taken in the absence of bubbles, under which conditions the pulses have temporal peak pressure amplitude (zero-peak) of around 25 kPa at 1 m from the source, and 7.2 kPa at the target as shown below in Figure 2.

The monitor hydrophone (placed 0.10 m in front of the source) shows the effect on the raw echo that results from the introduction of bubbles. Figure 7 shows a sequence of hydrophone records, arbitrarily chosen, which demonstrate the effect which the presence of bubbles have on the detectability of the target in the raw unprocessed echo of the first pulse of a number of consecutive TWIPS pairs. The bubbles provide clutter and variability.

The choice of the interval which separates the two pulses can affect the results. The TWIPS method assumes that there is insufficient change in the bubble population and target between the two pulses to degrade the technique. In the current experiment, the cloud in the beam will evolve through buoyant rise and size change in response to the steadily decreasing hydrostatic pressure. Therefore it might reasonably be expected that the upper limit for the inter-pulse interval (τ) will be based on the rate of bubble-cloud evolution. If scatterers in the acoustic field are allowed to move considerably during the pause between the two outgoing pulses, then the physical parameters dictating the scattering apparent in the first pulse return will not correlate well with those dictating the scattering within the second pulse return. In the tank, where the experiment has been designed to allow the bubbles to rise through buoyancy forces (and not under convective flow forces), an inter-pulse interval might be sufficiently long to degrade the TWIPS pulse if enough bubbles rose through a significant fraction of a wavelength (which at the operating frequency of 6 kHz used here, would be about 12 cm if the sound speed were around 1500 m s^{-1}).

Buoyant rise speeds in water are not simple, though in general the largest bubbles rise the most rapidly unless group effects occur [18, 16]. As can be seen from Figure 8, Stokes' law markedly underestimates the drag coefficient. From such considerations, an interpulse interval of 100 ms (the largest used in this paper) would present the TWIPS pulses with a sufficiently stable environment.

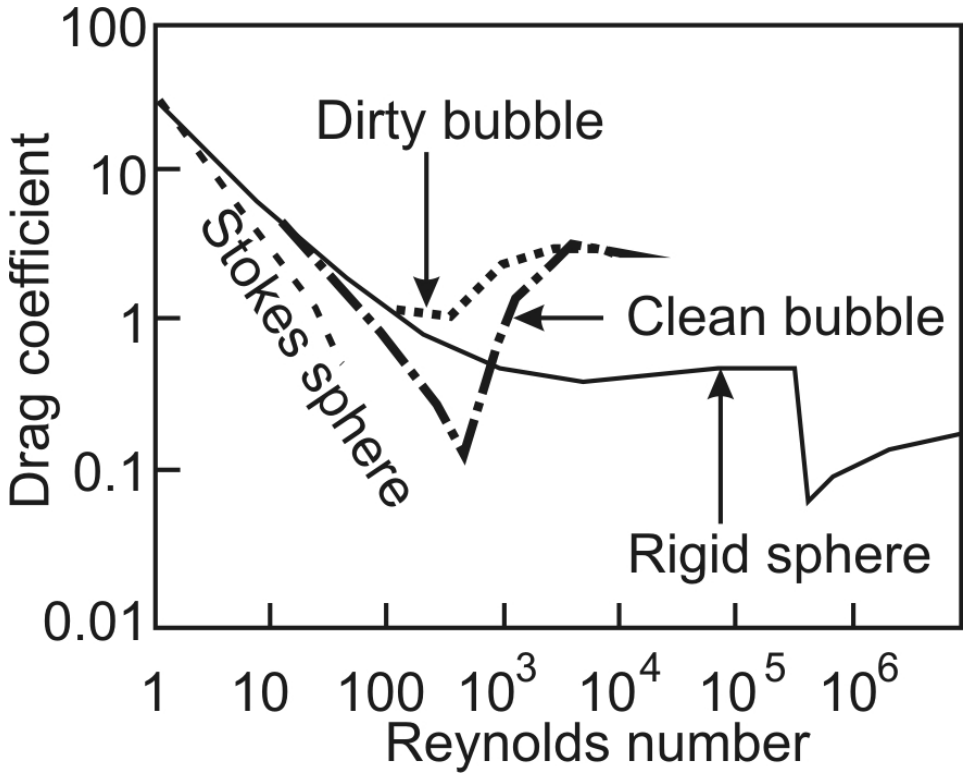

Figure 8. The variation in drag coefficient with Reynold's number for four types of sphere (copied from Leighton [17], which was based on data of Clift *et al.* [18].

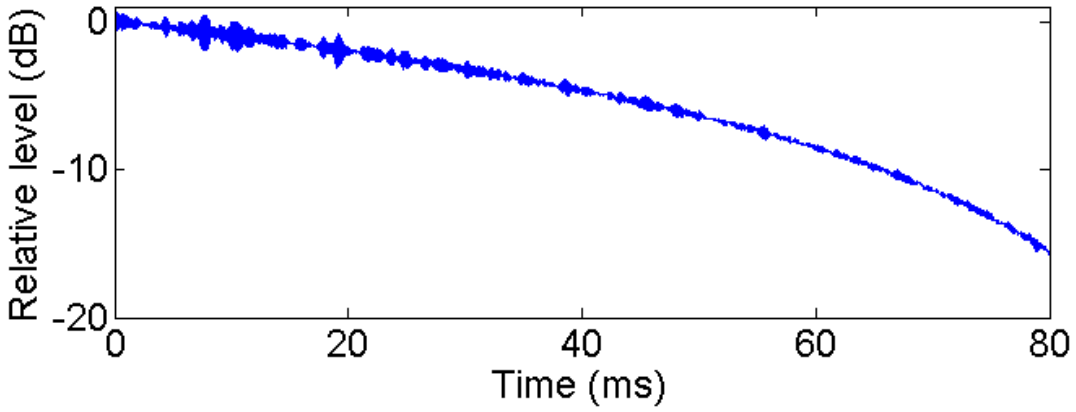

Figure 9. A reverberation curve for the test tank used for these TWIPS experiments. The T_{15} (reverberation time based extrapolation calculated from the rate of decay for the first 15 dB) for ISVR's A. B. Wood Tank at 6 kHz is 240 ms.

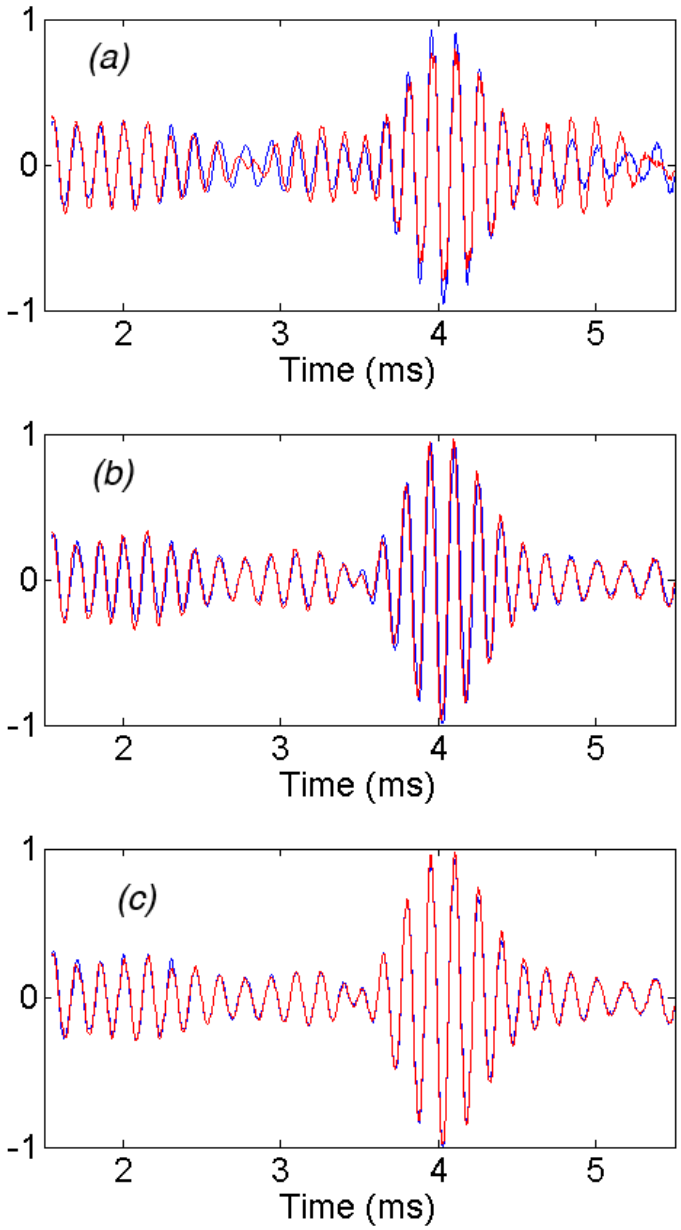

Figure 10. The effect of tank reverberation on pulse-pair matching (bubble-free conditions). In each plot, the initial outgoing pulse has been drawn in dark blue, and overlaid by the inverse of the second pulse (the second pulse is supposed to be identical to the initial pulse, except that it has reversed polarity with respect to it). Thus, if the second pulse is an identical opposite to the first, then in the plot shown, the red line should correlate perfectly with the blue line. The results are shown for three different pulse separation times, as follows: (a) τ = 20 ms (b) τ = 50 ms and (c) τ =100 ms. The target is visible as a broad peak in the region of 4 ms. Increasing agreement is gained as the interval increases (original in colour).

In a confined space such as a laboratory tank, the lower limit of the inter-pulse delay can be determined by the duration of the reverberation tail. The reverberation time of a space is defined as the amount of time it takes for level in a space resulting from an impulse to decrease by 60 dB. By analysing the decay of the first 15 dB, and extrapolating linearly, it is possible to estimate the reverberation time via the so-called T_{15}. In Figure 8, the reverberation tail for the tank is shown and has been smoothed after the method of Pierce [19]:

$$P_{rev}(t) = 10\log\left\{\frac{1}{T_{ref}}\int_{t}^{\infty}\frac{p(t')^2}{p_{ref}}dt'\right\} \quad (1)$$

where t is time, $p(t)$ is the pressure in the tank as a function of time, p_{ref} is an arbitrary reference pressure (chosen here to be the maximum pressure), T_{ref} is an arbitrary reference time, and $P_{\mathrm{rev}}(t)$ is the smoothed reverberation function.

From Figure 9 it can be seen that the T_{15} for the tank is 240 ms. Further, it can be seen that in order for the time-averaged sound pressure level to reduce by 10 dB following a single 6 kHz sound, the interpulse delay must be least 65 ms. That is, if two pings are played in close repetition within the tank, and a delay of less than about 65 ms is used, a detectable amount of reverberation from the first signal will still be present when the second signal is introduced into the water. This is demonstrated in Figure 10, where the acoustic returns from pulses projected with different inter-pulse intervals have been displayed to show clearly the interference resulting from reverberation.

In Figure 10, it is shown that the reverberant energy from the first pulse diminishes the correlation between the first and second pulses unless a delay of at least around 50 ms is used. It is unsurprising that Figure 10(a) shows poor correlation, as the reverberation curve shown in Figure 9 shows that the time-averaged reverberant energy within the tank is only reduced by about 3 dB after 20 ms.

To show the effect of reverberation interference on TWIPS results, the TWIPS experiment was conducted using the three different intervals used in Figure 10, specifically 20 ms, 50 ms, and 100 ms. The size of the bubble cloud was kept approximately constant during these experiments. As explained above, TWIPS functions as a result of the successful performance of two tasks: target highlighting and bubble-scattering suppression in the numerator (via P_-), and bubble scattering enhancement in the denominator (via P_+). Earlier experimental studies [3, 7-9] showed variability in the TWIPS2 signal in detecting a target within a bubble cloud, a feature which was apparent from the earlier simulations [3, 6]. Since TWIPS2 depends on the formation of the ratio P_-/P_+, this paper examines the sources of variability in P_+, how these could contribute the dynamic range of the TWIPS2 output, and the degree to which the effect varies with the inter-pulse time.

3. RESULTS

Figure 11-13 shows the performance of the TWIPS2 function P_-^2 / P_+ in detecting the target for, respectively, inter-pulse intervals of 20 ms, 50 ms and 100 ms. The colourscale in Figures 11-13 reflects the value of a TWIPS2 function as calculated by aligning and combining the echoes of the two TWIPS pulses. The target, when present, occurs at around t=3.75 ms. In Figures 11-13, 100 consecutive returns are stacked, such that a stationary target should appear as a vertical line (as do the later reflections from the walls of the tank, which are linear, e.g. the back wall reflection at ~6.75 ms).

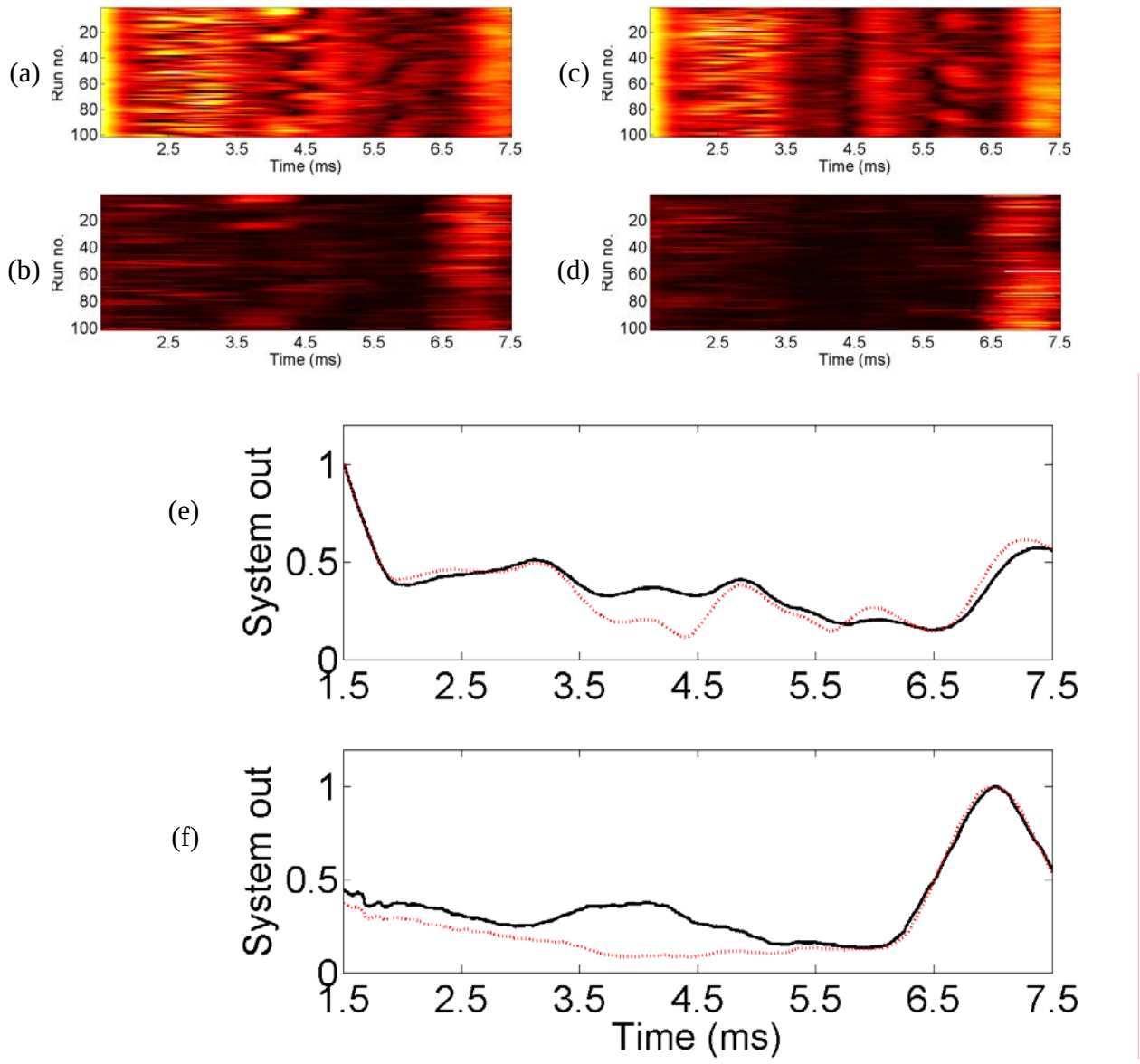

Figure 11. The output of the TWIPS2 function P_{-}^{2} / P_{+} when τ =20 ms, produced by stacking 100 consecutive echo time histories. In each of these figures, the target is located between 2.75 and 3.75 ms, and the bubble cloud between 1.5 and 2.5 ms. The echo from the back wall of the tank occurs at around 6.75 ms. Panels (a) and (b) show the case with the target present, and panels (c) and (d) show the case with the target absent. Panels (a) and (c) are produced using standard sonar processing. In panel (b) the same data as for 'a' has been reprocessed using TWIPS. In panel (d) the same data as for 'c' has been reprocessed using TWIPS. Panel (e) shows the means of the acoustic returns processed using the standard returns; Panel (f) shows the means of the acoustic returns processed using TWIPS. In (e) and (f), the black solid line shows the results when the target is present, and the red dotted line shows the results when the target was not present.

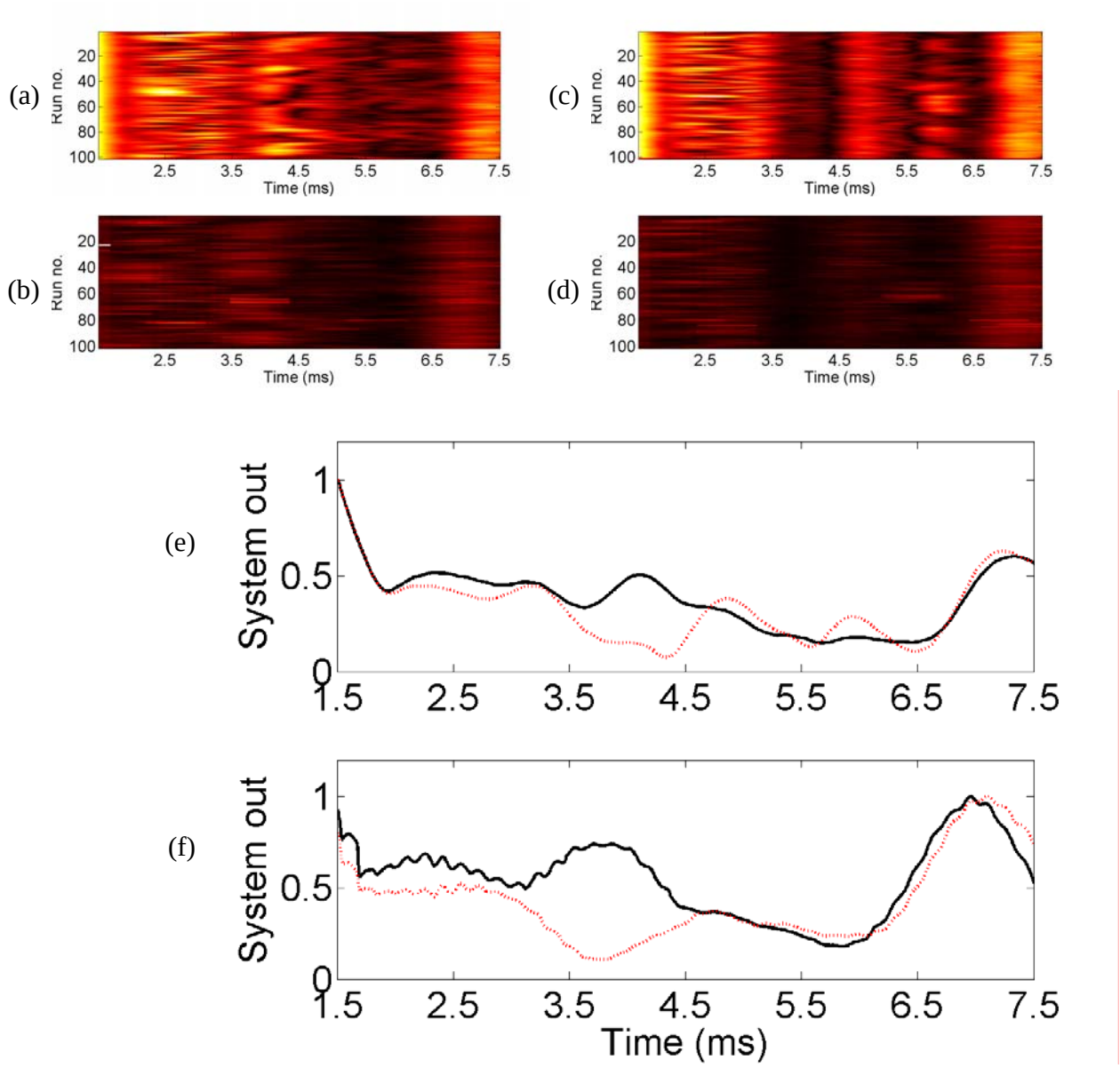

Figure 12. The output of the TWIPS2 function P_{-}^2 / P_{+} when τ =50 ms, produced by stacking 100 consecutive echo time histories. In each of these figures, the target is located between 2.75 and 3.75 ms, and the bubble cloud between 1.5 and 2.5 ms. The echo from the back wall of the tank occurs at around 6.75 ms. Panels (a) and (b) show the case with the target present, and panels (c) and (d) show the case with the target absent. Panels (a) and (c) are produced using standard sonar processing. In panel (b) the same data as for 'a' has been reprocessed using TWIPS. In panel (d) the same data as for 'c' has been reprocessed using TWIPS. Panel (e) shows the means of the acoustic returns processed using the standard returns; Panel (f) shows the means of the acoustic returns processed using TWIPS. In (e) and (f), the black solid line shows the results when the target is present, and the red dotted line shows the results when the target was not present.

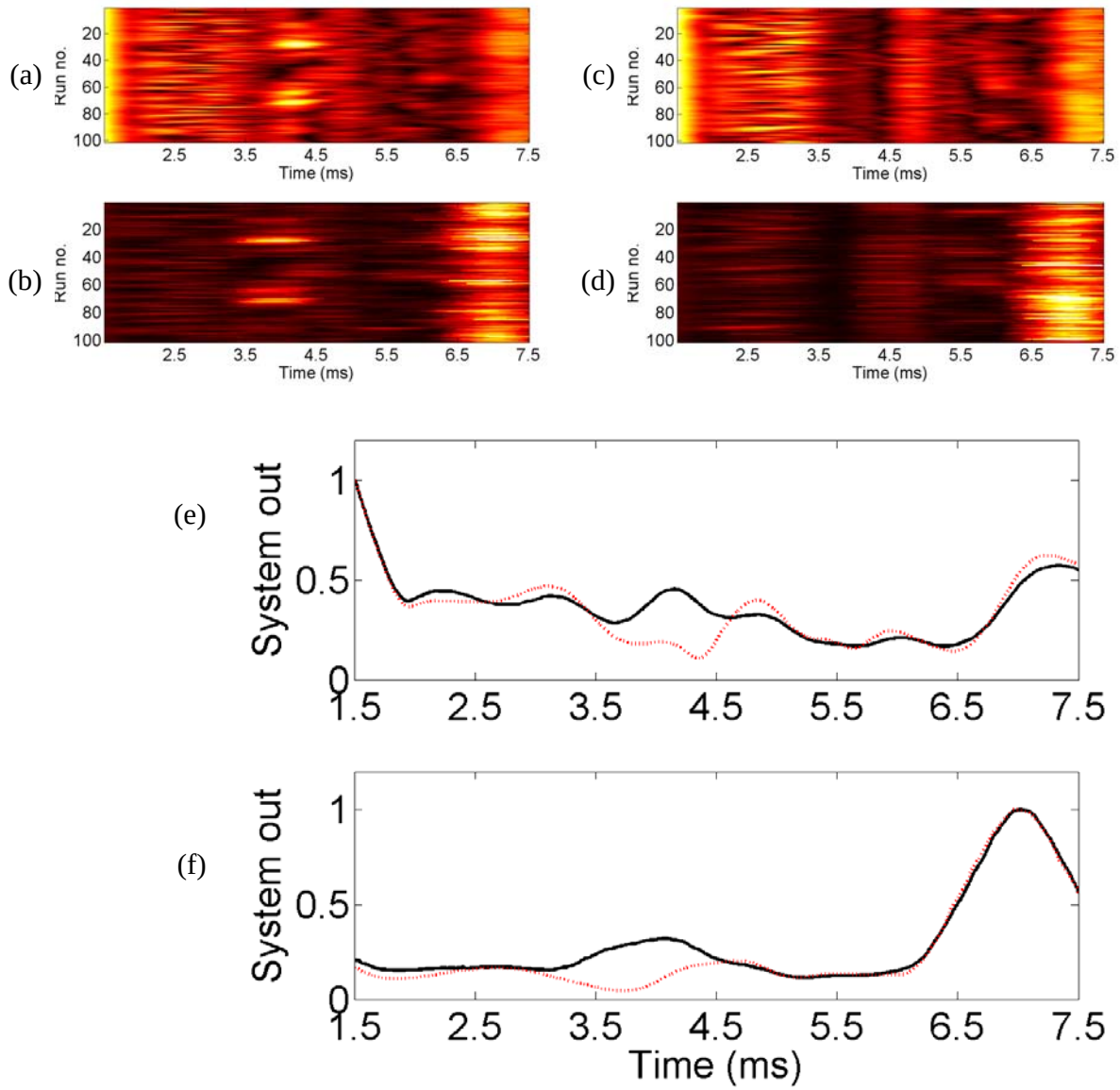

Figure 13. The output of the TWIPS2 function P_{-}^2 / P_{+} when τ =100 ms, produced by stacking 100 consecutive echo time histories. In each of these figures, the target is located between 2.75 and 3.75 ms, and the bubble cloud between 1.5 and 2.5 ms. The echo from the back wall of the tank occurs at around 6.75 ms. Panels (a) and (b) show the case with the target present, and panels (c) and (d) show the case with the target absent. Panels (a) and (c) are produced using standard sonar processing. In panel (b) the same data as for 'a' has been reprocessed using TWIPS. In panel (d) the same data as for 'c' has been reprocessed using TWIPS. Panel (e) shows the means of the acoustic returns processed using the standard returns; Panel (f) shows the means of the acoustic returns processed using TWIPS. In (e) and (f), the black solid line shows the results when the target is present, and the red dotted line shows the results when the target was not present.

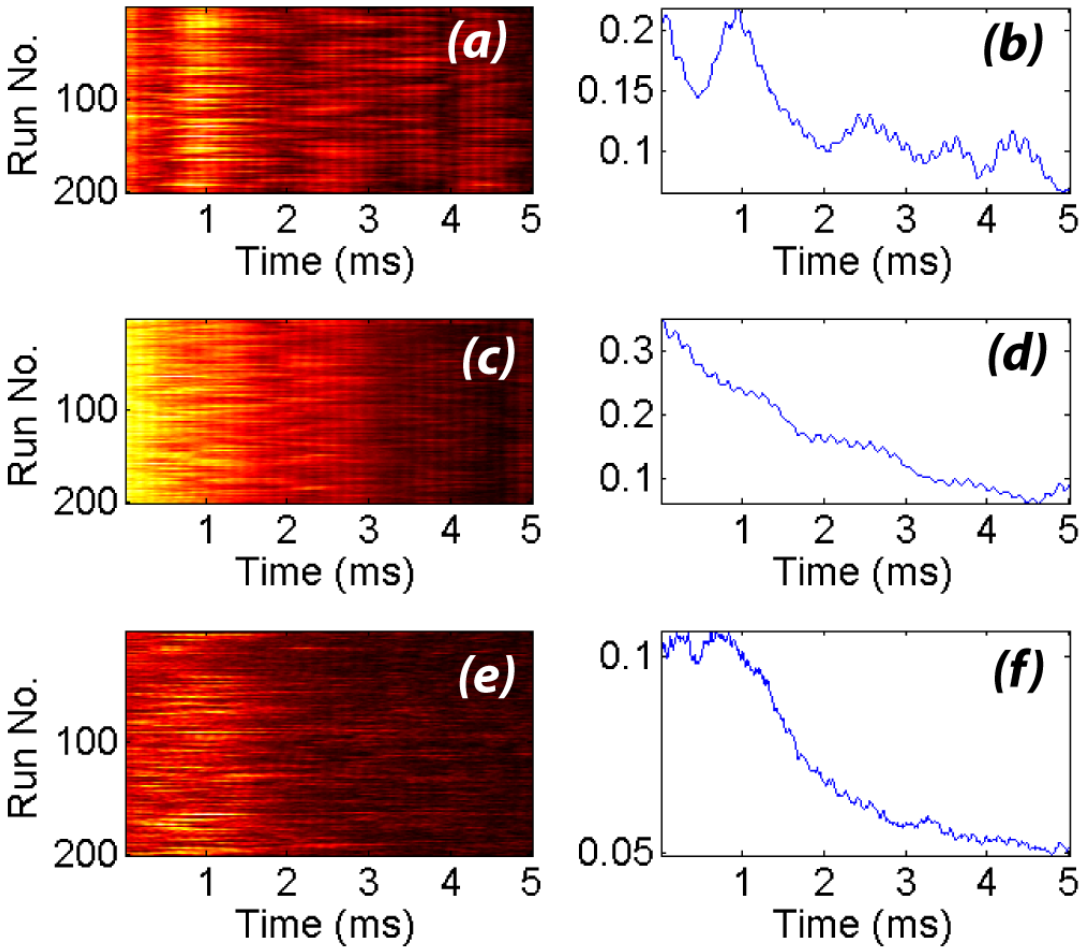

Figure 14. The effectiveness of P_+ (bubble contrast enhancement) with varying inter-pulse times. The bubble cloud is located between 0 and 2 ms, and the target is between 2 and 3 ms.
(a) Intensity plot, P_+ for 200 pulse pairs; τ =20 ms; (b) the median of all pulse pairs; τ =20 ms;
(c) Intensity plot, P_+ for 200 pulse pairs; τ =50 ms; (d) the median of all pulse pairs; τ =50 ms;
(e) Intensity plot, P_+ for 200 pulse pairs; τ =100 ms; (f) the median of all pulse pairs; τ =100 ms.

The ability of TWIPS to detect the target in the presence of bubble clutter increases with increasing inter-pulse interval in Figures 11-13. This is from the results of Figure 10, as the increased inter-pulse interval causes the second pulse in each TWIPS pair to reproduce the first pulse (in inverse form) with greater fidelity within the water column.

Figure 11 shows that when the interval is only 20 ms, the target gives a response which is approximately equal in amplitude to the response from the bubble cloud. The result obtained for 50 ms is better, but when 100 ms is used as an interval, the signal from the target is significantly higher in amplitude than that signal corresponding to scattering by the bubble cloud. This suggests that TWIPS is in fact a promising technique for identifying targets in bubble clouds.

The performance of the standard sonar reported in Figures 11, 12 and 13 is approximately unchanged. This is a result of the fact that the experiments were carried out in quick succession, with the bubble-cloud remaining at pseudo-steady state throughout the course of measurements. While standard sonar gives a difference between the with- and without target scenarios, the level corresponding to target scatter is approximately equal to the level corresponding to bubble scatter. In other words, it is not possible to distinguish between the target and the bubbles using standard sonar.

The echo from the back wall is always strong, because it is a strong scatterer. Note that at long ranges from the source, the field amplitude will be insufficiently great to generate the nonlinear bubble motions required to cause enhancement using TWIPS.

The results (particularly Figure 13(b)) also show the large dynamic range present in the TWIPS2 function (such that it appears that TWIPS2 only detects the target intermittently, a feature that could be offset human or dolphin sonar by the use of a train of clicks).

The source of the intermittency of the TWIPS2 signal will now be explored. The particular TWIPS2 function used in this paper is P_-^2 / P_+. Since the base of the ratio (P_+) is, at the position of the target, a small number formed by the subtraction of two large numbers, it is a prime candidate for the source of large dynamic fluctuations in TWIPS2.

This study will now explore whether the P_+ signal becomes more stable as the inter-pulse interval is varied. In Figure 14, the output of P_+ has been shown for varying inter-pulse times, τ. This P_+ signal, of course, enhances the bubbles and suppresses the target. The only filtering applied to the signal in Figure 14 was a high-pass filter used to eliminate DC offset and some 50 Hz mains leakage. When τ is insufficiently short, reverberation from the first pulse affects the return from the second pulse. Figures 14(a) and (b) show that this interference makes it difficult for P_+ to distinguish between linear and nonlinear scatterers for τ=20 ms. As a result, while there is the desired broad peak indicating a bubble cloud between 0 and 2 ms, there is an undesired peak in the target location between 2 and 3 ms. Figures 14(c) and (d) show that τ=50 ms functions much better as a bubble-cloud enhancer, but the gradual negative gradient from 0 ms to 3 ms does not show clearly where the bubble cloud lies. This gradual gradient presumably results from the fact that, whilst an interval of τ=50 ms allows the algorithm to enhance the bubble scatter, the target signal suppression is incomplete. Figures 14(e) and (f) show that an interval of τ=100 ms provides better discrimination. Figure 14(e) shows consistent bubble cloud scatter enhancement, and it is clear from Figure 14(f) that the target scatter has been significantly suppressed.

It must be emphasised that these results should theoretically be indicative of the types of problems that on might encounter when using TWIPS. However, the ideal inter-pulse interval τ will vary from location to location, as dictated by the bubble speeds and reverberation conditions encountered during a particular trial.

It has been shown that P_+ is capable of consistently enhancing bubble-scatter on the basis of nonlinear scattering, which is not surprising given the success of a similar technique in the biomedical field [10, 11]. However the effect of inter-pulse times shown here has particular implications in the oceanic environment. An alternative nonlinear signal component scattered by bubbles, which like P_+ is exploited to enhance the detection of bubbles and is used extensively in biomedical ultrasonics, is second-harmonic imaging. That method also requires the use of high-amplitude signals in a nonlinearly scattering environment, but requires only a single pulse. The return from that single pulse is then band-pass filtered to discriminate the second-harmonic

energy to show the location of nonlinear scatterers. The data used to generate Figure 14(a) were reprocessed to study the effectiveness of second-harmonic techniques in a pseudo-oceanic environment. To the best knowledge of the authors, this is the first time that second-harmonic bubble imaging has been applied in a large-scale setting.

The second-harmonic technique results shown in Figure 15 demonstrate that this technique is effective at suppressing the target scatter, but offers insufficient bubble-cloud enhancement. Observations during the experiment showed that the bubble cloud was located not just between 0 and 1 ms as suggested by Figure 15, but between 0 and 2 ms (a fact testified to by the results shown in Figures 14(e) and (f)). Compared to TWIPS, the cloud visibility obtained using the second-harmonic technique is limited; this is a result of bandwidth considerations. Recall that no frequency filters were used to enhance bubble scatter in TWIPS. This means that any anti-phase information present in the second pulse return, regardless of frequency, will give contrast enhancement when inverted and combined with the return from the first pulse. The second-harmonic technique, however, can only give contrast enhancement when the bubble scatter is within the frequency constraints of the band-pass filter. As the output signal is limited in length (8 cycles at 6.5 kHz), the outgoing pulse is broad in frequency content. While those bubbles closest to the acoustic driver will tend to be very active at twice the rate of the centre frequency, the remainder of the cloud will tend to be only weakly nonlinear, and may be relatively inactive within the limits of the filter. Therefore, limiting the bandwidth of the detector will limit the number of bubbles which can be perceived.

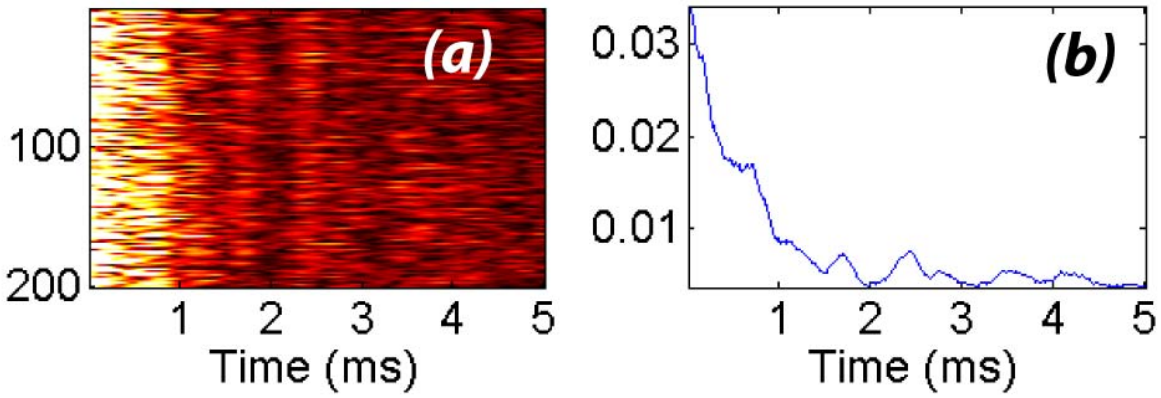

Figure 15. Second-harmonic imaging of a bubble cloud in the A B Wood Tank. The bubble cloud is located between 0 and 2 ms, and the target is located between 2 ms and 3 ms. (a) An intensity plot for 2 pulse-pairs. (b) Median of the 200 pings.

4. DISCUSSION

TWIPS has shown to be effective in empowering a man-made sonar to detect a target in bubbly water. Statistical studies (to investigate the ROC curve characteristics of TWIPS) and sea trials are currently underway. It is, however, interesting to return the question to the original stimulation for this work, which was the though-experiment that, if odontocetes were accomplishing echolocation in bubbly water, is there a way of designing a sonar to do such a task in the absence of any measurements of the acoustic signals odontocetes are employing in bubbly

water (a very different problem to that of testing biomimetic signals)? Given that TWIPS does detect objects in bubbly water, is there any evidence that ondontocetes are employing twin inverted pulses?

There is no conclusive evidence for this, but many intriguing clues that suggest that examination in the wild of certain shallow water species would be valuable, to answer the question one way or another. Of course in shallow water, normal incidence reflection from a plane air-water interface will introduce a phase inversion into the reflected pulse. However it is not so easy to produce a scenario in the wild whereby the direct signal from an odontocete to a hydrophone, is followed a short time later by a phase inverted version of that pulse with the same amplitude (e.g. because of surface ripples, spreading losses etc.). It would be a somewhat simpler task to design a source which produced a phase-inverted second pulse at source, using a pressure release interface close to the source.

Tab. 1: Species to which a search for TWIPS-like pulses might be targeted (with sources for evidence referenced: Dawson, 1988 [20]; Goodall *et al.*, 1988 [21]; Kamminga and Wiersma, 1981 [22]; Evans *et al.*, 1988 [23]; Li *et al.*, 2005 [2424]; Awbrey *et al.*, 1979 [25]; Au, 1993 [26]). Note: Awbrey *et al.* made the first high frequency recordings of Dall's porpoise, but the authors of this paper were unable to obtain this report.

Genus	Species	Primary Habitat	Evidence	Sources
Cephalorhynchus	Hector's dolphin, *Cephalorhynchus hectori*	Coastal New Zealand, often in estuaries	Have been recorded (single hydrophone) sustained sets of equal-amplitude pulses with constant separation times	Dawson (1988) kindly provided recordings
	Commerson's dolphin, *Cephalorhynchus commersonii*	Coastal East Argentina, South Chile, & Indian Ocean		Goodall *et al.* (1988); Kamminga and Wiersma (1981); Evans *et al.* (1988)
	Heaviside dolphin, *Cephalorhynchus heavisidii*	West coast of South Africa	Near-shore habitats, but the authors have found no recordings	
	Chilean/Black dolphin, *Cephalorhynchus eutropia*	Coastal Chile		
Phocoena	Finless Porpoise, *Neophocoena phocaena*	Coastal Asia.	Equal amplitude phase inverted pulses which Li *et al.* attribute to surface reflections	Li *et al.* (2005)
	Dall's porpoise, *Phocoena dalli*	Coastal, warm temperate to sub-arctic waters of the Northern Pacific Ocean.	Some evidence of multiple pulses but no evidence of equal amplitude	Evans *et al.* (1988), Awbrey *et al.* (1979).
	Harbour porpoise, *Phocoena phocoena*	Coastal waters of subarctic & cool temperate North Atlantic & North Pacific. Often inshore.		Au (1993)

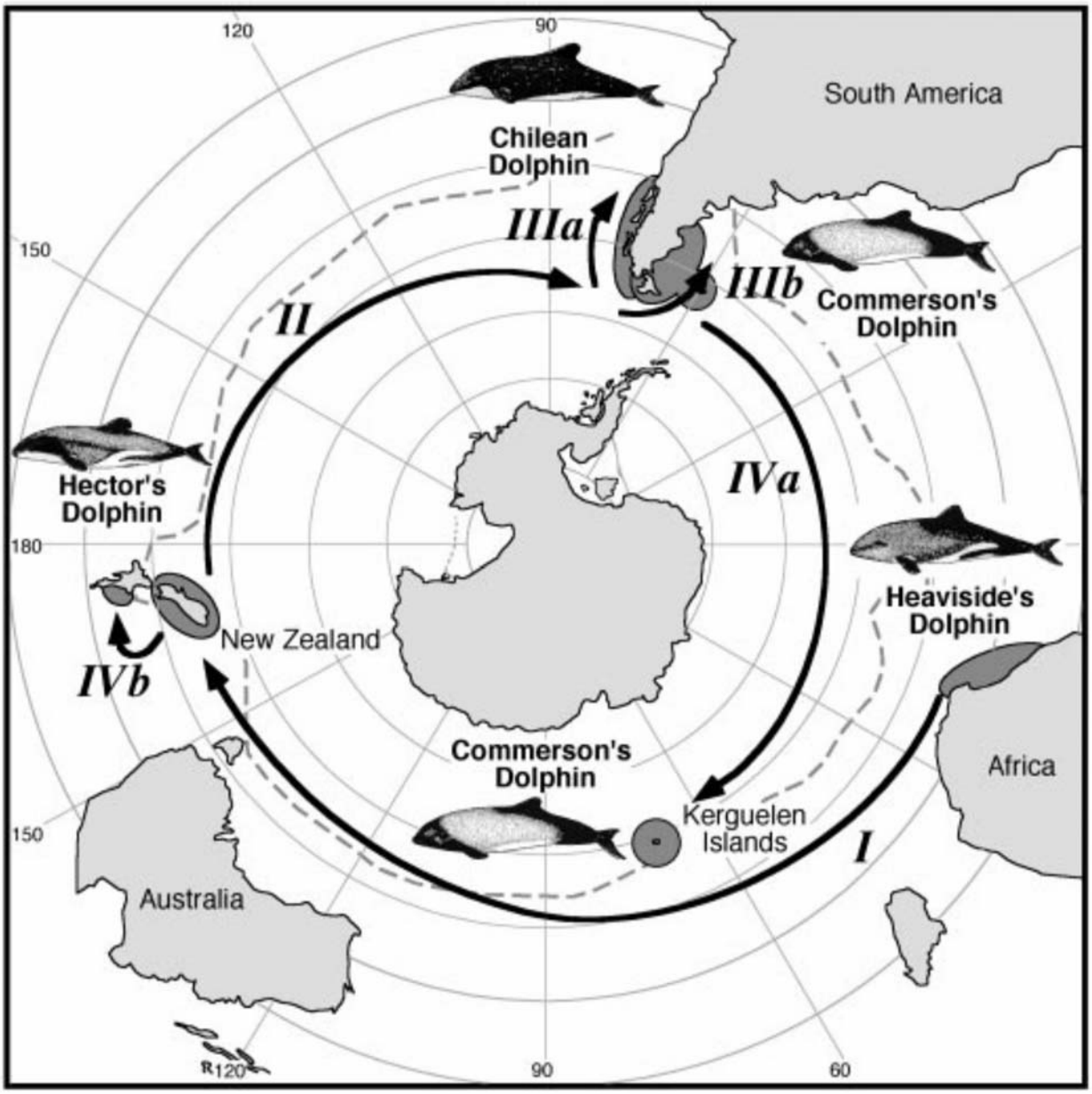

Figure 13. Map of the progression of *Cephalarynchus* as determined from maternal DNA (from Pilcher *et al.* [27]).

A major hindrance to this study is the lack of suitable data from the field. Table 1 lists those dolphins and porpoises (all belonging to the genera *Cephalarynchus* and *Phocoena*) which form suitable candidates for such an examination, and the reasons for this. The primary habitats for all members of these genera are shallow waters - the same waters for which TWIPS was invented as a sonar solution. Their evolutionary path has been traced using mitochondrial DNA (Figure 13). According to Pilcher *et al*. [27] "Our results suggest that coastal, depth-limited odontocetes are prone to population fragmentation, isolation and occasionally long-distance movements, perhaps following periods of climatic change…"The *Cephalorhynchus* originated in South Africa and spread east to New Zealand (I) then continued east to South America (II). The South American dolphin population moved northwards with glaciation of Tierra del Fuego to form the Chilean dolphin (IIIa) and Commerson's dolphin (IIIb)…. More recently (perhaps in the last 10 000 years) a population of Commerson's dolphins has founded a population at the Kerguelen Islands (IVa)…"".

5. ACKNOWLEDGEMENTS

No sponsor has agreed to fund these, or previous, TWIPS studies. As such the authors have been very grateful to Dr Justin Dix for his assistance in providing a source with the required capabilities, and to Anne-Marie Liszczyk for assistance with the tank experiments.

REFERENCES

1. T. G. Leighton, "From seas to surgeries, from babbling brooks to baby scans: The acoustics of gas bubbles in liquids," *International Journal of Modern Physics B,* Vol. 18(25), 3267-3314, 2004.
2. T. G. Leighton, "Nonlinear bubble dynamics and the effects on propagation through near-surface bubble layers," In *High-Frequency Ocean Acoustics,* Eds. M.B. Porter, M. Siderius, and W. Kuperman, (American Institute of Physics Melville, New York) *AIP Conference Proceedings* Vol. 728, pp. 180-193, 2004.
3. T. G. Leighton, P. R. White, D. C. Finfer, "Target Detection in Bubbly Water," *International patent application number* PCT/GB2006/002335; European Patent Application No. 06755621.7 National Phase of PCT/GB2006/002335; claiming priority from UK patent application GB 0513031.5, University of Southampton, 2005.
4. T. G. Leighton, P. R. White, D. C. Finfer, S. D. Richards, "Cetacean acoustics in bubbly water," *Proc. First Int. Conf. on Underwater Acoustic Measurements, Technologies and Results,* J.S. Papadakis and L. Bjorno, eds. (Crete), pp. 891-898, 2005.
5. T. G. Leighton, P. R. White, D. C. Finfer, "Bubble acoustics in shallow water: possible applications in Nature," *Proc. Int. Conf. on Boundary influences in high frequency, shallow water acoustics* (Bath), pp. 433-440, 2005.
6. T. G. Leighton, D. C. Finfer, P. R. White, "Bubble acoustics: What can we learn from cetaceans about contrast enhancement?" *Proc. 2005 IEEE International Ultrasonics Symposium* (Rotterdam) pp. 964-973, 2005.
7. T. G. Leighton, D. C. Finfer, P. R. White, "Sonar which penetrates bubble clouds," *Proceedings of the Second International Conference on Underwater Acoustic Measurements, Technologies and Results,* J.S. Papadakis and L. Bjorno, eds (Heraklion, Crete), 555-562, 2007.

8. T. G. Leighton, D. C. Finfer, P. R. White, "Cavitation and cetacean," *Revista de Acústica*, Vol. 38(3-4), 37-81, 2007.
9. T. G. Leighton, D. C. Finfer, P. R. White, "Cavitation and cetacean," *Proceedings of the 19th International Congress of Acoustics* (Madrid) Paper PL003, pp. 1-31, 2007.
10. D. H. Simpson, Ting Chin Chien, P. N. Burns, "Pulse inversion Doppler: a new method for detecting nonlinear echoes from microbubble contrast agents," *IEEE Transactions on Ultrasonics, Ferroelectrics and Frequency Control*, Vol. 46, 372-382, 1999.
11. P. N. Burns, S. R. Wilson, D. H. Simpson, "Pulse Inversion Imaging of Liver Blood Flow: Improved Method for Characterizing Focal Masses with Microbubble Contrast," *Invest. Radiol.* Vol. 35, 58-71, 2000.
12. D. G. H. Coles, T. G. Leighton, "Autonomous spar-buoy measurements of bubble populations under breaking waves in the Sea of the Hebrides," *Proceedings of the Second International Conference on Underwater Acoustic Measurements, Technologies and Results*, J.S. Papadakis and L. Bjorno, eds (Heraklion, Crete), 543-548, 2007.
13. D. M. Farmer, S. Vagle, "Waveguide propagation of ambient sound in the ocean-surface bubble layer," *J. Acoust. Soc. Am*. Vol. 86,1897-1908, 1989.
14. D. M. Farmer, S. Vagle, "Bubble measurements using a resonator system," In *Natural physical processes associated with sea surface sound*, T.G. Leighton (ed.), University of Southampton, UK, pp. 155-162, 1997.
15. N. D. Breitz, H. Medwin, "Instrumentation for *in-situ* acoustical measurements of bubble spectra under breaking waves," *J. Acoust. Soc. Am.* Vol. 86, 739-743, 1989.
16. C. E. Brennen, *Cavitation and Bubble Dynamics*, (Oxford University Press, Oxford), 1995.
17. T. G. Leighton, *The Acoustic Bubble*, (Academic Press, London), pp. 115-124, 1994.
18. R. Clift, J. R. Grace, M. E. Weber, *Bubbles, Drops and Particles*, (Academic Press, San Diego), 1978.
19. A.D. Pierce, *Acoustics: An introduction to its physical principles and applications*, (Acoustical Society of America, New York), 1994.
20. S. M. Dawson, "The high-frequency sounds of Hector's dolphins *Cephalorhynchus hectori*," *Rep. Int. Whal. Commn. Spec. Issue*. Vol. 9, 339-344, 1988.
21. R. N. P. Goodall, K. S. Norris, A. R. Galeazzi, J. A. Oporto, I. S. Cameron, "On the Chilean dolphin, *Cephalorhynchus eutropia* (Gray, 1846)," *Rep. Int. Whal. Commn. Spec. Issue*, pp. 197-257, 1988.
22. C. Kamminga, H. Wiersma H, "Investigations on cetacean sonar II. Acoustical similarities and differences in *odontocete* sonar signals," *Aquatic Mammals*, Vol. 8, pp. 41-62, 1981.
23. W. E. Evans, F. T. Awbrey, H. Hackbarth, "High frequency pulses produced by free-ranging Commerson's dolphin (*Cephalorhynchus commersonii*) compared to those of Phocoenids," In: *Biology of the genus Cephalorhynchus.* Edited by R.L.B. Jr., G.P. Donovan. Cambridge: International Whale Commision, pp. 173-181, 1988.
24. S. Li, K. Wang, D. Wang, T. Akamatsu, "Echolocation signals of the free-ranging Yangtze finless porpoise (*Neophocaena phocaenoides asiaeorientialis*)," *Journal of the Acoustical Society of America* Vol. 117, 3288-3296, 2005.
25. F. T. Awbrey, J. C. Norris, A. B. Hubbard, W. E. Evans, The bioacoustics of the Dall's porpoise salmon drift net interaction (San Diego), 1979.
26. W. W. L. Au: *The Sonar of Dolphins* (Springer-Verlag, New York), 1993.

27. F. B. Pichler, D. Robineau, R. N. P. Goodall, M. A. Meÿer, C. Olivarría, C. S. Baker, "Origin and radiation of Southern Hemisphere coastal dolphins (genus *Cephalorhynchus*)," *Molecular Ecology*, Vol. 10, 2215-2223, 2001.